



Department of Physics & Astronomy
Experimental Particle Physics Group
Kelvin Building, University of Glasgow,
Glasgow, G12 8QQ, Scotland

Telephone: +44 (0)141 339 8855 Fax: +44 (0)141 334 9029

GLAS-PPE/97-01
November 6, 2018

Recent Results from the study of QCD and Jets at HERA

L.E. Sinclair¹

for the ZEUS and H1 Collaborations

*Talk presented at the Lake Louise Winter Institute, Particles and the Universe,
Lake Louise, Alberta, Canada, February 1997.*

Abstract

The HERA experiments H1 and ZEUS have recently presented a number of interesting results from studies of the hadronic final state produced in ep collisions. These studies have focussed on deep inelastic scattering events and on the photoproduction of jets, and also on the comparison of the final states produced in these two regimes. Some of these results are reviewed here.

arXiv:hep-ex/9706018v1 24 Jun 1997

¹e-mail: sinclair@desy.de

1 Introduction

Analyses of the distribution of final state hadrons¹ in ep scattering events can provide tests of the theory of strong interactions, quantum chromo-dynamics (QCD). These studies have yielded information on the value and running of α_s , on the physics of parton shower evolution, on the structure of the photon and proton and on the underlying parton scattering dynamics. There are too many recent results from H1 and ZEUS to attempt a complete review here. Instead I will concentrate on the measurement of fragmentation functions in deep inelastic scattering (DIS) [1], some results from the measurement of jet cross sections in photoproduction [2, 3], a study of prompt photon production [4] and some results from the comparison of the hadronic final state produced in deep inelastic scattering with that produced in photoproduction [5, 6]. These results pertain to data collected in the 1994 and 1995 periods of data taking, during which HERA provided collisions of 27.5 GeV positrons against 820.0 GeV protons, delivering about 3 nb^{-1} and 6 nb^{-1} of luminosity respectively.

2 Hadronic Final State in Deep Inelastic Scattering

In the leading order quark parton model of DIS, the incident positron scatters from a quark in the proton via the exchange of a boson whose negative invariant mass squared is denoted Q^2 . The quark carries a fraction x_{Bj} of the proton's longitudinal momentum and energy into the hard subprocess. This simple picture is sufficient to allow the appreciation of the results presented here.

2.1 Fragmentation Functions

To characterize the parton showering and subsequent hadronization which determine the distribution of hadrons in the final state, the distribution of the scaled momentum x_p is measured. The scaled momentum is defined as the magnitude of a hadron's momentum relative to the maximum momentum available to it, $x_p = p_{\text{HADRON}}/p_{\text{MAX}}$. The measurement of scaled momentum distributions is carried out in the "Breit" or "brickwall" frame where $p_{\text{MAX}} = -Q/2$. In this frame the current hemisphere in DIS is directly comparable to one hemisphere in an e^+e^- annihilation event where the centre-of-mass energy E^* would represent the energy scale, Q , and $p_{\text{MAX}} = E^*/2$.

In fact a variable transformation is commonly made to $\xi = \ln(1/x_p)$ which has an approximately Gaussian distribution. The distribution of ξ is called a fragmentation function. As an example, fragmentation functions in two bins of Q^2 are shown in Figure 1 for data taken by H1 during the

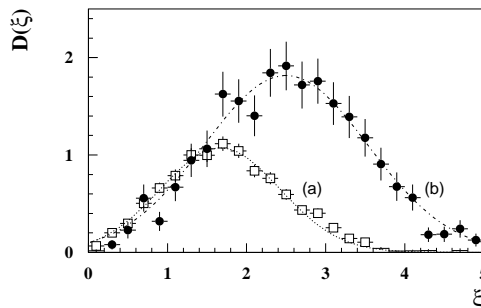


Figure 1: Fragmentation functions for (a) $12 < Q^2 < 80 \text{ GeV}^2$ and (b) $Q^2 > 100 \text{ GeV}^2$. Gaussian fits to the distributions are superimposed.

1993 running period [7]. The data support the intuitive expectation that as Q^2 increases, the average charged multiplicity should increase, $\langle x_p \rangle$ should decrease, and $\langle \xi \rangle$ should increase.

To quantify the Q^2 evolution of $\ln(1/x_p)$, a Gaussian fit of the ξ distribution has been made for several different Q bins. The resulting fit parameters for the peaks of the Gaussian distributions, ξ_{peak} ,

¹In the ep world it is common to refer to all of the final state particles other than the scattered lepton as the "hadrons".

are shown in Figure 2 [1]. The data are consistent with a QCD inspired picture of fragmentation in which ξ_{peak} is expected to scale approximately linearly with $\ln Q$. A pure phase space model would entail a slope of unity in the dependence of ξ_{peak} on $\ln Q$ while a fit to the data yield 0.75 ± 0.05 . Therefore the data prefer coherent fragmentation as predicted by QCD. (See also reference [7] and references therein.)

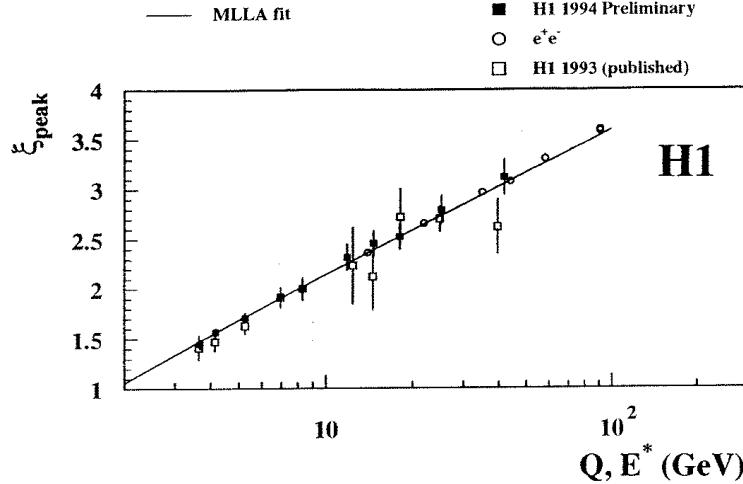


Figure 2: Peak values of the Gaussian fit to the $\xi = \ln(1/x_p)$ distribution versus Q for H1 1993 (open squares) and H1 1994 (filled squares) data. The line shows a linear fit to the data. Also shown is the corresponding ξ distribution parameter versus E^* for e^+e^- data (circles).

Results for the evolution of the ξ_{peak} fit parameter with E^* for e^+e^- data are also shown in Figure 2. The consistency of the e^+e^- data with the ep data supports the application of a single universal treatment of parton showering and hadronization.

3 Photoproduction of Jets

Deep inelastic scattering processes (Figure 3(a)) are characterized by rather high values of the negative squared four momentum of the boson (usually a photon), $Q^2 > \mathcal{O}(1) \text{ GeV}^2$. In photoproduction on

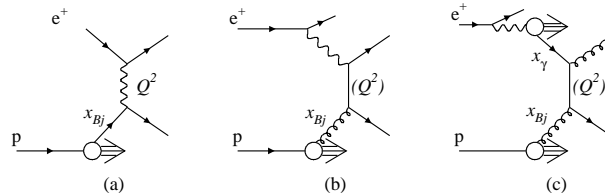


Figure 3: Diagrams for DIS (a) and direct (b) and resolved (c) photoproduction.

the other hand the photon is nearly real. When jets are produced in photoproduction, their transverse energy sets the energy scale of the process, also often represented by Q^2 .

At leading order there are two photoproduction processes which lead to the production of high transverse energy jets. In “direct” photoproduction the photon participates directly in a hard scattering with a parton from the proton as illustrated in Figure 3(b). In “resolved” photoproduction (Figure 3(c)) the photon first fluctuates into a hadronic state a parton from which enters the hard subprocess. It is therefore necessary to introduce another Bjorken scaling variable, denoted x_γ , which represents the fraction of the photon’s momentum which is carried by the interacting parton.

3.1 Jet Cross sections

ZEUS has measured the dijet photoproduction cross section differential in the average jet pseudorapidity, $d\sigma/d\bar{\eta}$, for events with at least two $E_T^{\text{JET}} > 6$ GeV jets [3]. By making the requirement that $x_\gamma > 0.75$, we effectively examine the direct photoproduction cross section [8]. The results are shown in Figure 4(a) where three different jet finders have been used to define the cross section. EUCELL

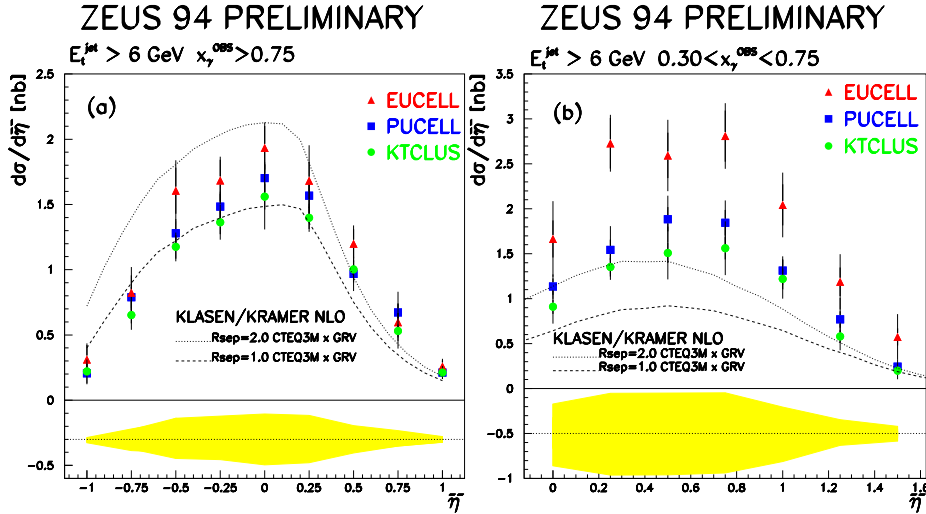


Figure 4: Dijet photoproduction cross section, $d\sigma/d\bar{\eta}$, for (a) $x_\gamma > 0.75$ and (b) $0.30 < x_\gamma < 0.75$. The different symbols show the measured cross section using three different jet finding algorithms. The curves show NLO calculations of the cross section using the CTEQ3M proton parton distributions and the GRV photon parton distributions for two different values of the R_{sep} parameter (see text). (The shaded band shows the correlated uncertainty on the absolute energy scale of the detector.)

and PUCELL are cone algorithms which satisfy the Snowmass convention [9]. The difference between them illustrates the sensitivity of the measurements to the choice of seed particle and the treatment of overlapping cones. KTCLUS is a cluster jet finding algorithm [10].

The results are compared to next to leading order (NLO) predictions for the cross sections using the KTCLUS algorithm and two different values of the R_{sep} parameter [11]. (R_{sep} defines the farthest distance in pseudorapidity and azimuth that two partons can have from one another and still be combined into one jet [12].) The prediction shown by the dashed line may be directly compared with either the PUCELL or KTCLUS cross sections which are equivalent at NLO and have an effective R_{sep} value of 1. The theory provides a reasonably good description of both the normalization and shape of the measured distribution. In EUCELL the effective value of R_{sep} is not precisely defined but is in the range 1.5→2. The theory is therefore able to describe the spread of the cross sections due to the different jet finding algorithms.

The situation is considerably worse for the resolved photon processes. The cross section $d\sigma/d\bar{\eta}$ for $0.30 < x_\gamma < 0.75$ is shown in Figure 4(b). Here the NLO calculation for the KTCLUS algorithm (dashed line) does not describe the measured KTCLUS cross section. Also the cross section suffers more variation under change of jet algorithm and this variation is not describable by the NLO calculation. However it must be noted that much of the uncertainty due to the photon structure is contained in the resolved sample and that also the higher order processes which are not included in the fixed order calculation would show up at low x_γ .

It is possible to define an effective parton distribution of the photon, $f_{i/\gamma} = \sum(q + \bar{q}) + 9/4g$, which can be measured in photoproduction [13]. Note that in contrast to deep inelastic $e\gamma$ experiments which only determine the quark content of the photon, the HERA γp measurements are sensitive also to the gluonic term of $f_{i/\gamma}$. By comparison of measured parton level cross sections with the PYTHIA [14] Monte Carlo leading order prediction H1 have extracted the effective parton distribution of the photon

in three bins of x_γ as a function of the hard scattering scale, p_t^2 (the square of the partonic transverse momentum). [2] This is shown in Figure 5.

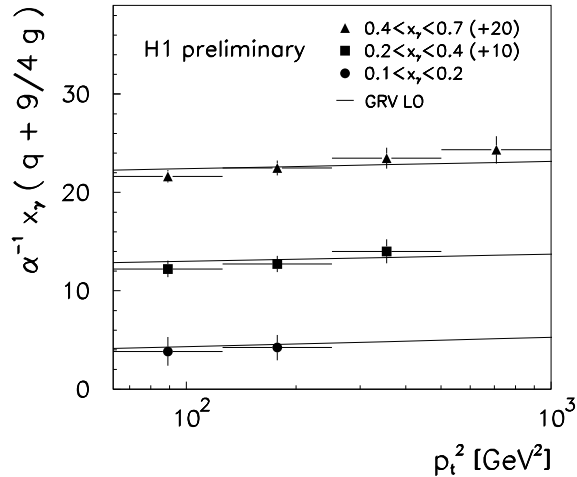


Figure 5: The symbols show the photon parton density versus p_t^2 in three bins of x_γ . The curves represent the photon parton density calculated using the GRV-LO parton distribution functions.

The data are consistent with a logarithmic rise of $f_{i/\gamma}$ with p_t^2 . We recall that a calculation of the quark content of the photon from the box diagram $\gamma\gamma^* \rightarrow q\bar{q}$ yields the form $F_2^\gamma \text{ box} = a(x_\gamma) + b(x_\gamma) \log p_t^2$ [15]. It is therefore interesting to speculate whether the logarithmic rise of $f_{i/\gamma}$ with p_T^2 reveals a component of the resolved photon which results directly from a splitting of the photon into a $q\bar{q}$ pair. This has been called the “anomalous” component in contrast to that part of the photon’s structure which behaves as though the photon has fluctuated into a vector meson.

3.2 Prompt Photon Production

A particularly interesting photoproduction event topology occurs when a high transverse energy photon takes the place of one of the jets. Such processes are called prompt photon processes. These events provide a clean QCD laboratory for the study of quark jet showering and fragmentation and for the measurement of the quark content of the resolved photon. This is also the best process for the study of initial-final state QCD coherence. In direct photoproduction there is a single flow of colour from the incoming to the outgoing quark, in contrast to the situation in generic dijet production where many different possible colour flows contribute to each event topology.

To select a sample of prompt photon events a jet and an isolated electromagnetic energy deposit in the ZEUS barrel calorimeter with no associated charged particle found in the tracking chamber, are required. However some dijet events, where one jet consists largely of a single π^0 or η , can pass this selection. This contribution can be understood using a Monte Carlo simulation as shown in Figure 6(a) [4]. The fraction of the electromagnetic shower energy which is contained in the highest energy calorimeter cell is denoted f_{max} . Photons give signals with higher values of f_{max} than the π^0 background and it is possible to describe the measured distribution of f_{max} by allowing for a small π^0 component. This also allows for an admixture of η ’s.

The x_γ distribution for prompt photon events after subtraction of the π^0 background is shown in Figure 6(b). The distribution is roughly consistent in shape and normalization with a leading order QCD prediction. Most of the events have high values of x_γ and are therefore associated with direct prompt photon production. We look forward to a larger sample of prompt photon events with the 1996 and 1997 delivered luminosities.

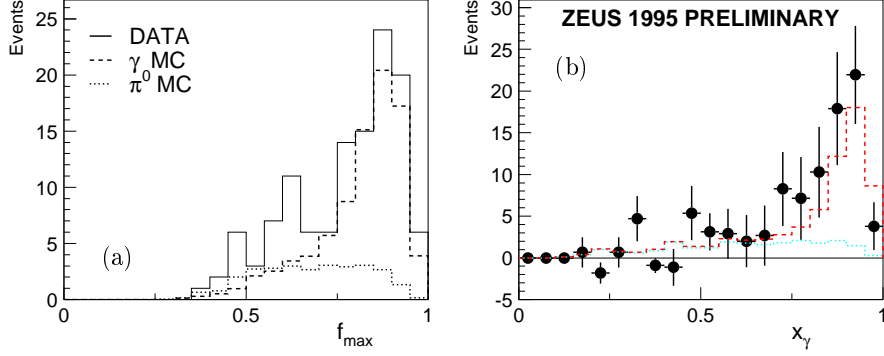


Figure 6: (a) The distribution of f_{\max} for the data (solid histogram), the simulated prompt photon events (dashed histogram) and the simulated π^0 background (dotted histogram). In (b) the black dots show the x_γ distribution for prompt photon events after background subtraction. The dashed histogram shows the expectation from the PYTHIA Monte Carlo simulation. The dotted histogram shows the simulated x_γ distribution separately for the (leading order) resolved component.

4 Comparison of Deep Inelastic Scattering and Photoproduction

Two interesting recent results compare the hadronic final states in deep inelastic scattering and photoproduction. These studies are particularly appealing to the experimentalist since it is possible to make some interpretation of the data which does not rely on a comparison of the data to theory.

4.1 Transverse Energy Flow

H1 has measured the flow of transverse energy in the hadronic centre of mass frame across a large range of Q^2 , as shown in Figure 7 [5]. The hadronic centre of mass frame pseudorapidity, η^* , is defined

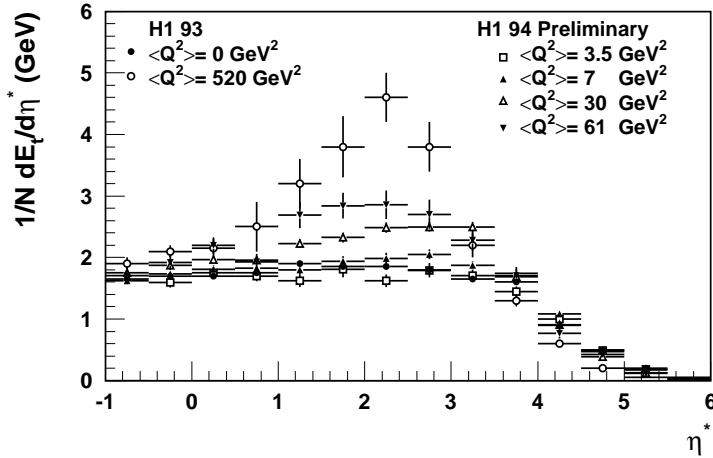


Figure 7: Average transverse energy, E_T , in bins of the hadronic centre of mass frame pseudorapidity, η^* , and $\langle Q^2 \rangle$.

such that the proton direction is negative so the current region is at positive η^* .

The E_T in the current region of course grows with $\langle Q^2 \rangle$. However the remarkable feature of this distribution is that the mean transverse energy in the central region, $\eta^* \sim 0$, is practically independent of Q^2 from the soft photoproduction region, $\langle Q^2 \rangle = 0$, up to the very deep inelastic region, $\langle Q^2 \rangle = 520 \text{ GeV}^2$. H1 therefore find that there is a smooth transition in the development of the global flow of transverse energy between the photoproduction and DIS regimes.

4.2 Jet Shapes

A complementary result from ZEUS concerns the internal structure of jets [6]. The jets are found using a cone algorithm with jet radius $R = 1$. The jet shape parameter, $\psi(r)$, has been defined as the fraction of the jets transverse energy which is contained within a smaller concentric cone of radius r . This is

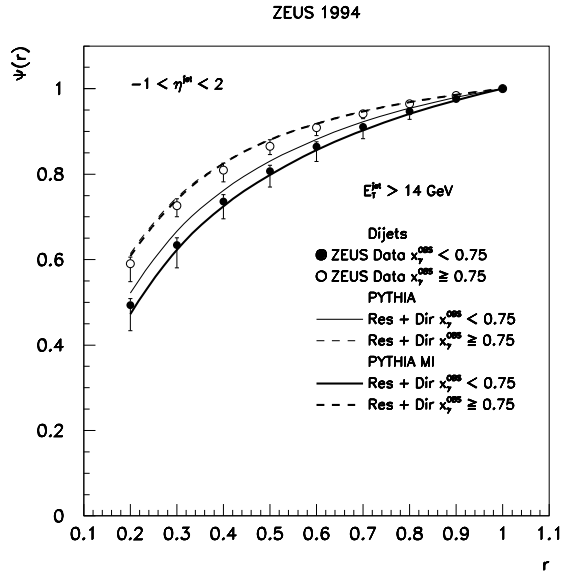


Figure 8: Jet shapes in dijet photoproduction for high (open circles) and low (black dots) x_γ samples. The PYTHIA predictions for the low and high x_γ regions are shown by the solid and dashed lines respectively. Thicker lines show the PYTHIA predictions where multiple interactions between the constituents of the photon and proton have been allowed.

shown in Figure 8 for a sample of photoproduction events which have two jets of $E_T^{\text{JET}} > 14 \text{ GeV}$ and $-1 < \eta^{\text{JET}} < 2$. The jet shape is shown separately for direct and resolved photon events. The jet shape for the $x_\gamma \geq 0.75$ sample is narrower than the shape of the jets for the resolved photon sample. This effect is reproduced by the parton shower Monte Carlo model PYTHIA. Allowing for secondary interactions between the photon and proton remnant particles in the simulation improves the description of the $x_\gamma < 0.75$ data.

One can speculate that the observed difference in the high and low x_γ jet shapes is due primarily to the colour charge of the parton which initiates the jet. In direct photoproduction this parton is predominantly a quark whilst in resolved photoproduction the jets are much more often initiated by gluons. If the direct photoproduction jets are narrower than the resolved photoproduction jets because of the predominance of quark jets, then one would expect the jet shapes of the high x_γ events to be comparable to jet shapes in DIS. This is indeed the case as shown in Figure 9 [6]. The high x_γ jet shape is shown in four bins of η^{JET} and is found to be comparable with the jet shape for DIS events ($Q^2 > 4 \text{ GeV}^2$) having at least one $E_T > 14 \text{ GeV}$ jet [6].

5 Conclusions

Quantum chromodynamics is a successful theory. For a number of years it has been clearly established that in the perturbative regime QCD matrix elements describe the dynamics of parton scattering. Here it is shown that ep scattering provides the means to perform detailed tests of the QCD inspired models for parton showering and hadronization. These models, as implemented in Monte Carlo event generators, are able to describe the measured observables. There is also strong evidence that the fragmentation process has a universal nature given the similarity of the hadronic final states in e^+e^- and in DIS events as well as in DIS and photoproduction events.

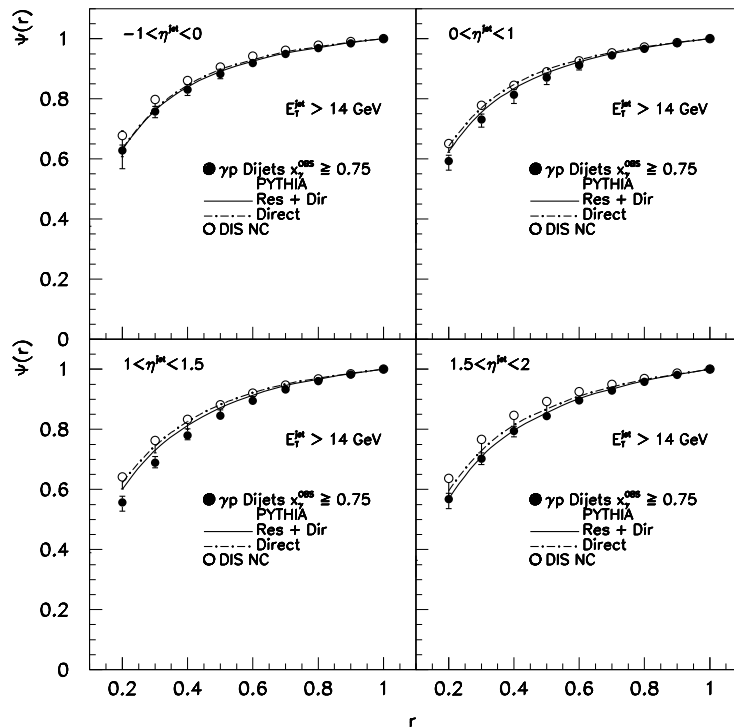


Figure 9: Jet shape in direct photoproduction (dark dots) compared with jet shape in DIS (light dots) in four bins of η^{JET} . The data are not corrected for detector effects and are compared with PYTHIA Monte Carlo predictions to which a full simulation of the ZEUS detector has been applied. The prediction for the the high x_γ jet shape is shown by the dark line and the prediction for the pure leading order direct processes is shown by the light line.

Acknowledgments

My thanks to the members of the H1 and ZEUS collaborations who have performed the analyses discussed here. The organizers of the Lake Louise Winter Institute are to be congratulated for having succeeded to provide a most enjoyable and stimulating atmosphere for the exchange of ideas.

References

- [1] S. Aid *et al* (H1 Collaboration), contribution pa02-072 to *XXVIII International Conference on High Energy Physics*, July 1996, Warsaw.
- [2] S. Aid *et al* (H1 Collaboration), contribution pa02-080 to *XXVIII International Conference on High Energy Physics*, July 1996, Warsaw.
- [3] M. Derrick *et al* (ZEUS Collaboration), contribution pa02-040 to *XXVIII International Conference on High Energy Physics*, July 1996, Warsaw.
- [4] M. Derrick *et al* (ZEUS Collaboration), contribution pa02-042 to *XXVIII International Conference on High Energy Physics*, July 1996, Warsaw.
- [5] S. Aid *et al* (H1 Collaboration), contribution pa02-073 to *XXVIII International Conference on High Energy Physics*, July 1996, Warsaw.
- [6] M. Derrick *et al* (ZEUS Collaboration), contribution pa02-043 to *XXVIII International Conference on High Energy Physics*, July 1996, Warsaw.

- [7] S. Aid *et al* (H1 Collaboration), *Nucl. Phys. B* **445**, 3 (1995).
- [8] M. Derrick *et al* (ZEUS Collaboration), *Phys. Lett. B* **348**, 665 (1995).
- [9] J. Huth *et al* in *Proceedings of the DPF 1990 Summer Study on High Energy Physics, Snowmass, Colorado*, ed. E. L. Berger, World Scientific, 134 (1992).
- [10] S.Catani, Yu.L.Dokshitzer, M.H.Seymour and B.R.Webber, *Nucl. Phys. B* **406**, 187 (1993).
- [11] M. Klasen and G. Kramer, *Z. Phys. C* **72**, 107 (1996).
- [12] S.D.Ellis, Z.Kunszt and D.E.Soper, *Phys. Rev. Lett.* **69**, 3615 (1992).
- [13] B.L.Combridge and C.J.Maxwell, *Nucl. Phys. B* **239**, 429 (1984).
- [14] H.-U.Bengtsson and T. Sjöstrand, *Comp. Phys. Comm.* **46**, 43 (1987); T. Sjöstrand, CERN-TH.6488/92, (1992).
- [15] E. Witten *Nucl. Phys. B* **120**, 289 (1977).